Research Article | Vol. 27, No. 18 / 2 September 2019 / Optics Express 25251
Optics EXPRESS

Highly reconfigurable hybrid laser based on an integrated nonlinear waveguide

A. Aadhi,[1,9] Anton V. Kovalev,[2,9] Michael Kues,[3] Piotr Roztocki,[1] Christian Reimer,[1,4] Yanbing Zhang,[1] Tao Wang,[1,5] Brent E. Little,[6] Sai T. Chu,[7] Zhiming Wang,[5] David J. Moss,[8] Evgeny A. Viktorov,[2,10] and Roberto Morandotti[1,2,5,11]

[1]*Institut National de la Recherche Scientifique - Énergie Matériaux Télécommunications, 1650 Boulevard Lionel-Boulet, Varennes, Québec J3X 1S2, Canada*
[2]*ITMO University, Birhzevaya Liniya 14, 199034 St. Petersburg, Russia*
[3]*Hannover Center for Optical Technologies, Leibniz University Hannover, Nienburger Str. 1, 30167 Hannover, Germany*
[4]*John A. Paulson School of Engineering and Applied Sciences, Harvard University, Cambridge 02138, USA*
[5]*Institute of Fundamental and Frontier Sciences, University of Electronic Science and Technology of China, Chengdu 610054, Sichuan, China*
[6]*Xi'an Institute of Optics and Precision Mechanics, Chinese Academy of Sciences, Xi'an 710119, China*
[7]*City University of Hong Kong, Tat Chee Avenue, Hong Kong, China*
[8]*Centre for Micro Photonics, Swinburne University of Technology, Hawthorn, Victoria 3122, Australia*
[9]*These authors contributed equally to this work.*
[10]*evviktor@gmail.com*
[11]*morandotti@emt.inrs.ca*

Abstract: The ability of laser systems to emit different adjustable temporal pulse profiles and patterns is desirable for a broad range of applications. While passive mode-locking techniques have been widely employed for the realization of ultrafast laser pulses with mainly Gaussian or hyperbolic secant temporal profiles, the generation of versatile pulse shapes in a controllable way and from a single laser system remains a challenge. Here we show that a nonlinear amplifying loop mirror (NALM) laser with a bandwidth-limiting filter (in a nearly dispersion-free arrangement) and a short integrated nonlinear waveguide enables the realization and distinct control of multiple mode-locked pulsing regimes (e.g., Gaussian pulses, square waves, fast sinusoidal-like oscillations) with repetition rates that are variable from the fundamental (7.63 MHz) through its 205th harmonic (1.56 GHz). These dynamics are described by a newly developed and compact theoretical model, which well agrees with our experimental results. It attributes the control of emission regimes to the change of the NALM response function that is achieved by the adjustable interplay between the NALM amplification and the nonlinearity. In contrast to previous square wave emissions, we experimentally observed that an Ikeda instability was responsible for square wave generation. The presented approach enables laser systems that can be universally applied to various applications, e.g., spectroscopy, ultrafast signal processing and generation of non-classical light states.

1. Introduction

Mode-locked lasers are quintessential for photonics technologies and find widespread application in fields as diverse as spectroscopy, materials processing, biomedical research, and optical communications [1–3]. Since their first realizations, mode-locking techniques have evolved to enable the generation of laser field outputs with adjustable pulse duration, average power, pulse energy, and repetition rate [4]. As a coherent pulse train corresponds to a phase-locked

#364423 https://doi.org/10.1364/OE.27.025251
Journal © 2019 Received 8 Apr 2019; revised 30 Jul 2019; accepted 31 Jul 2019; published 22 Aug 2019

Optics EXPRESS

comb of optical modes in the spectral domain, mode-locking techniques generally operate by coherently redistributing energy among the cavity modes via sideband generation. This is either accomplished actively through modulators, or passively via nonlinear saturating elements [5]. Passive mode-locking techniques are preferred over active ones, since external and complex synchronized driving circuits are not required. In addition, passive mode-locking schemes deliver ultrafast and/or high repetition rate optical pulse trains [6]. Various nonlinear saturable absorbers based on semiconductor materials have been developed and investigated to realize passive mode-locking with low operational power thresholds, wavelength independency, and high modulation depths [4].

Notably, the nonlinear amplifying loop mirror (NALM) architecture (consisting of a fiber loop with a nonlinear element) can provide a power-dependent transfer function, analogously to a saturable absorber [7]. Figure-eight NALM laser configurations (see below for a detailed description) have been among the most influential fiber-based techniques for the generation of short pulses (e.g. down to few tens of fs) with large spectral bandwidths (tens of nm) [8,9]. Remarkably, NALMs have recently also been shown to enable the generation of the narrowest-bandwidth Kerr nonlinearity mode-locked pulses to date (i.e. in the ns regime) [10]. Moreover, variations of NALM architectures have produced e.g. Gaussian pulses [10], square wave pulses (via a so-called dissipative soliton resonance effect) [11], as well as higher harmonic pulse trains [12]. Different pulse profiles are suited for specific applications in assorted fields of science and technology. For example, ubiquitous Gaussian pulse profiles can be used, e.g., for ground-penetrating radars, sensitive measurements of material optical properties and for fluorescence scanning microscope implementations [13–15]. Higher harmonic trains of Gaussian pulses are beneficial for high speed lightwave communication and optical clocks [16]. In addition, harmonic mode-locking has recently found application in increasing photon pair generation rates for quantum technologies [17]. Similarly, less common square wave pulses can be employed to perform optical gating, fast signal processing, as well as optical switching [18]. Square wave pulses generated via a dissipative soliton resonance [19] are characterized by very low duty cycles, which can hinder some beneficial applications. For example, a 50% duty cycle is useful for clocking because it enables utilizing both rise and fall edges as clock triggers and hence, minimizes the clock skew [20]. Therefore, the dynamic control over pulse profiles provided by NALM configurations would offer the advantage of using a single, simple system. However, achieving a versatile range of pulse dynamics from one device typically requires the precise control of various parameters independently, such as gain and loss, and further requires careful engineering of both the nonlinearity and the dispersion properties of the laser cavity [19,21]. It therefore remains a challenge to achieve versatile output pulse profiles from a single, let alone a low-complexity, laser system.

Here, we theoretically predict and experimentally observe coherent emission of i) mode-locked (ML) pulses, ii) harmonically mode-locked (HML) pulses, iii) square waves (SWs), iv) modulated square waves (MSWs), v) spike square waves (SSWs) and vi) fast field oscillations (FOs) from a novel NALM configuration, externally tunable through polarization control and amplification. Due to its intrinsic hybrid fiber-based/integrated configuration, the system is affordable, practical and robust, allowing its use in field operations.

2. Laser scheme

The considered configuration is based on a figure-eight NALM (see Fig. 1). In a typical realization, the input in the NALM stage is divided, by means of a beam splitter, into two counter-propagating fields. Due to the different sequence of amplification and nonlinearity, the counter-propagating fields experience a phase difference, which leads to an intensity-dependent interference at the beam splitter and hence to an optical field coupling into the output port of the NALM (rather

Optics EXPRESS

than a fiber mirror operation). The NALM thus acts as an artificial saturable absorber and can therefore enable mode-locked laser operation [7].

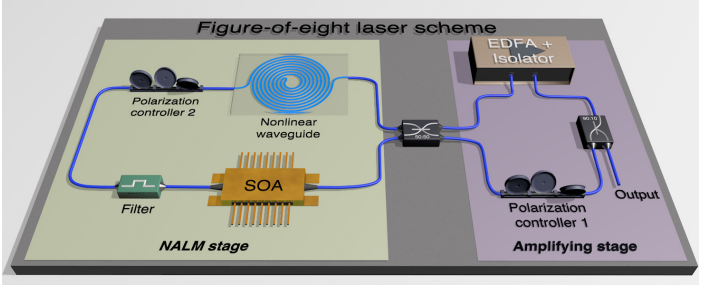

Fig. 1. Schematic of the laser system for variable pulse profile emissions: An integrated nonlinear waveguide, a bandpass filter (200 GHz at 1550 nm), and a semiconductor optical amplifier (SOA) were employed in the NALM stage. A beam splitter and an EDFA with a built-in optical isolator were used in the amplifier stage. The polarization controllers in both (NALM and amplifying) stages are used to manipulate the nonlinear phase via the control of both linear losses and effective nonlinearity, leading to tunability between different operational regimes.

In our configuration, a semiconductor optical amplifier (SOA, Inphenix INC: IPSAD1507C-5213) was used in the NALM section to provide gain and thus intensity difference for two propagation directions at the spiral waveguide entrance. Importantly, the system employed an integrated waveguide (with a length of 45 cm confined in a 2×2 mm^2 footprint; for a description of the device see, e.g., [22–24]) as a nonlinear element. The waveguide features a group velocity dispersion of $\beta_2 = -10$ ps^2/km (~8 ps/(nm·km)) at 1550 nm and provides a sufficiently high third-order nonlinearity (with a nonlinear constant of 220 W^{-1} km^{-1}), which can introduce a large nonlinear phase shift over a short propagation length. An erbium-doped fiber amplifier (EDFA, Keopsys) was used to compensate the losses inside the cavity and force unidirectional operation by means of a built-in optical isolator. The NALM stage also employs a bandpass filter (200 GHz bandwidth at 1550 nm center wavelength) to limit the optical operation frequency. Combined with the moderate cavity length of ~40 m and reasonably low dispersion of the used optical components, this allows to neglect the influence of dispersion in our system (in contrast, e.g., to the strong dispersion required for operation in the dispersive soliton resonance regime). Note that the nonlinear response and losses associated to the waveguide, featuring a rectangular cross section, are polarization dependent [24] due to different bending losses for the quasi TE and TM modes of the waveguide [25]. This allowed us to use polarization controllers to regulate the nonlinear phase difference between the counterpropagating fields and the experienced losses. As a result, the ability to adjust nonlinearity and losses enabled us to access mode-locked regimes with different pulse profiles and patterns. These can be varied from traditional mode-locking to square wave pulses having 50% duty cycle, as well as their harmonics, in a controlled manner.

It should be emphasized that using a spiral non-resonant waveguide response instead of an integrated high-Q microring resonator [10] provides a much higher optical bandwidth for the system, which leads to more versatility in terms of operating parameters. In addition to the strict limitations imposed by the narrow resonant frequencies of the microring (150 MHz) and its polarization anisotropy, a high-Q resonator has a certain light storage time leading to non-instantaneous coupling between the two counter-propagating fields in the NALM. Although beneficial to the outstanding coherence properties of the pulse train reported in [10], these characteristics do not allow the same level of precise control and accurate attenuation of the

Optics EXPRESS

dynamical processes experimentally shown in the arrangement based on an integrated spiral waveguide.

3. Theoretical model for NALM architecture

The complex laser dynamics are governed by the combined effects of gain, loss, and nonlinearity. Benefiting from the negligible impact of dispersion in the cavity loop, we modeled the system by means of a delay differential equation (DDE) derived using a lumped-element approach (previously employed to describe mode-locked operation in lasers [26]). Note that a simple DDE model designed for an analytical treatment of the dynamics in the long time-delay limit has been recently proposed by some of the authors in [27]. In this paper, we explore a more sophisticated, 'ad hoc' model tailored to describe the experimental configuration presented above (see also Appendix), and focus on the control of the NALM nonlinear response and corresponding dynamics. Here, we specifically target hysteresis as well as a variety of mode-locked states and their harmonics.

The model reads:

$$\begin{aligned}\Gamma^{-1}\dot{E}(\tau) + E(\tau) = \tfrac{\sqrt{\kappa}}{2}\exp\tfrac{1}{2}[(1-i\alpha)G_{\mathrm{SOA}}(E(\tau-1))+\\ G_{\mathrm{EDFA}}(E(\tau-1))]\Phi(\tau-1)E(\tau-1),\end{aligned} \tag{1}$$

where the time variable $\tau \equiv t/T$ is normalized to the cold cavity round trip time T; $E(\tau)$ is a slow-varying normalized complex field amplitude inside the cavity defined at the point just before the beam splitter (see Fig. 1); Γ is the dimensionless filter bandwidth corresponding to the narrowest band-limiting element of the system (here the bandpass filter); κ is the total field intensity attenuation per round trip due to the linear non-resonant losses inside the cavity (adjustable with the polarization controllers); and α is the linewidth enhancement factor of the SOA [28]. The active medium dynamics in the SOA are fast (~1 ns) compared to the cavity round trip time of the NALM laser (~0.1 μs). Therefore, we can adiabatically eliminate the SOA material response and consider $G_{\mathrm{SOA}}(F) = J_{\mathrm{SOA}}/[1 + S_{\mathrm{SOA}}|F|^2]$ as a description of the cumulative saturable gain of the SOA. Here J_{SOA} is the SOA small signal gain parameter and S_{SOA} is inversely proportional to the SOA saturation intensity. For simplicity, we consider the EDFA gain in a similar manner: $G_{\mathrm{EDFA}}(F) = J_{\mathrm{EDFA}}/[1 + S_{\mathrm{EDFA}}|F|^2]$ with the corresponding parameters J_{EDFA}, and S_{EDFA}. Since the dynamics of the EDFA are much slower (~100 μs) than the NALM laser cavity round trip time, the EDFA is considered to provide linear gain, which we accounted by taking $S_{\mathrm{EDFA}} \ll S_{\mathrm{SOA}}$. $\Phi(\tau)$ is the nonlinear field response of the, NALM given by:

$$\Phi(\tau) = \left\{1 - \exp\left[\frac{-i\gamma|E(\tau)|^2}{2}(\exp G_{\mathrm{SOA}}(E(\tau)) - 1)\right]\right\}\exp\frac{-i\gamma|E(\tau)|^2}{2}, \tag{2}$$

where γ is an effective total third-order nonlinear coefficient. This function is a product of two terms. The first term represents the interference between two counterpropagating fields at the output of the NALM after the beam splitter, where $-i\gamma|E(\tau)|^2(\exp G_{\mathrm{SOA}}(E(\tau)) - 1)/2$ accounts for the nonlinear phase difference between the two field directions which can be controlled by means of the SOA gain. The second term is the phase shift without this attenuation. As it directly follows from Eq. (2), in the absence of nonlinearity ($\gamma = 0$) as well as for $G_{\mathrm{SOA}}(E(\tau)) = 0$, the destructive interference at the beam splitter, caused by equal phase shifts for both clockwise and counter-clockwise paths, does not allow light to be coupled from the output port of the NALM into the amplifying stage.

We classify the laser performance in relation to the SOA gain and cavity losses, and distinguish two cases based on the NALM response in Eq. (2). For low values of the SOA gain, the NALM response amplitude $|\Phi(\tau)|$ gradually increases with the intensity of the cavity field, and saturates

Optics EXPRESS

at larger intensities (see Fig. 2(a)). The NALM response is, therefore, identical to that of a saturable absorber with very high contrast, which leads to a stable laser off state for the entire parameter range of the SOA since the perturbations of the laser-off state are effectively damped. The dynamics observable when integrating Eq. (1), are similar to the standard mode-locked operation of a common semiconductor laser with a long cavity [29,30]. In such case, the near transform-limited, pedestal-free fundamental mode-locked pulse train and its harmonics are not self-starting and are bistable to the laser off state. The pulse shape essentially corresponds to a Gaussian profile.

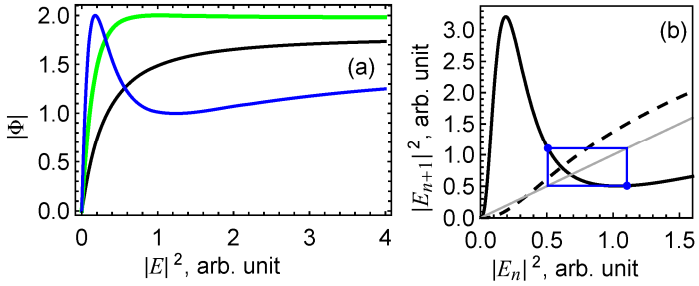

Fig. 2. **(a)** Amplitude response of the NALM as a function of the field intensity for different SOA gain values: $J_{SOA} = 1.5$ (black), $J_{SOA} = 2.25$(green), $J_{SOA} = 3.0$ (blue). **(b)** An illustration of the full system response function in the limit of a large filter bandwidth Γ as given by the right-hand side of Eq. (3) (black). The blue line demonstrates an example (for $J_{SOA} = 3.13$) of a stable period-two orbit of the map which corresponds to a periodic switching between two intensity values (1.1→0.5→1.1→. . . ; the grey line is $|E_n|^2 = |E_{n+1}|^2$). The dashed black line illustrates the right-hand side of Eq. (3) for $J_{SOA} = 1.5$, when period-two orbits and therefore SWs do not exist. The other parameters are: $\kappa = 0.3$, $S_{SOA} = 1$, $\gamma = 3$, $J_{EDFA} = 1.5$, $S_{EDFA} = 0.1$.

The character of the NALM response drastically changes for larger SOA gain values due to an increased phase asymmetry between propagation directions introduced inside the NALM, leading to a more complex response with multiple extremes (see Fig. 2(a)). In this case, the system behavior is essentially reminiscent of the Ikeda model [31,32], which is characterized by the appearance of period-two square waves (with respect to the cavity round trip time) of the continuous dynamic system through the so-called Ikeda instability, manifested by the appearance of the period doubling bifurcation of the corresponding discrete dynamic system.

In the limit of a large Γ, the model Eqs. (1)–(2) can be written as a discrete map relating the field intensity $|E_{n+1}|^2$ at the $(n+1)^{\text{th}}$ cavity round trip to that of the precedent n^{th} round trip:

$$|E_{n+1}|^2 = \kappa \exp\left(\frac{J_{SOA}}{1+S_{SOA}|E_n|^2} + \frac{J_{EDFA}}{1+S_{EDFA}|E_n|^2}\right)\times \sin^2\left(\frac{1}{4}\gamma|E_n|^2\left(1-\exp\frac{J_{SOA}}{1+S_{SOA}|E_n|^2}\right)\right)|E_n|^2. \tag{3}$$

The interference character of the NALM response is manifested by the sine function which is standard for Ikeda-like models, yet is attenuated by the nonlinear amplification of the SOA and EDFA. The map in Eq. (3) therefore results from two essential processes in the device: combined nonlinear amplification in the SOA and EDFA, and nonlinear loss modulation by the NALM. The result is the Ikeda instability of the cw solution, leading to switching between two intensity states. This occurs on a period-two timescale with respect to the cavity round trip time, and therefore leads to the supercritical appearance of mode-locked SW pulses with 50% duty cycle. We attribute the appearance of the SW regime of the laser to the balance between the highly nonlinear NALM response, gain, and loss inside the cavity. In turn, it leads to the appearance of

Optics EXPRESS

the stable period-two orbit of this map (see Fig. 2(b)). Harmonics of this period-two orbit are also possible, and appear as an odd number fraction of the period-two orbit cycle as described in [30,31], see our further discussion in this paper.

In order to explore the diverse nonlinear dynamics of the system, we numerically integrate Eq. (1) while slowly changing the SOA gain parameter J_{SOA}. To simplify the numerical integration, we considered the number of longitudinal modes determined by the filter width Γ to be 20. This parameter plays a crucial role in the laser dynamics, i.e. increasing the mode number will cause more complex states and pulse profiles as well as a higher number of coexisting multistable states. The SOA gain J_{SOA} is the control parameter for the NALM response variation used in the numerical calculations. Here the bifurcation diagram with gradually increasing J_{SOA} is presented in Fig. 3(a). For low J_{SOA} values, the bifurcation diagram shows that the system operates in a mode-locked regime (fundamental (ML) or harmonic (HML), Figs. 3(b) and 3(c)). Increasing J_{SOA} leads to the appearance of quasiperiodic pulsations followed by chaotic oscillation. In this respect, the NALM hybrid laser mimics the behavior of a long cavity laser with a saturable absorber.

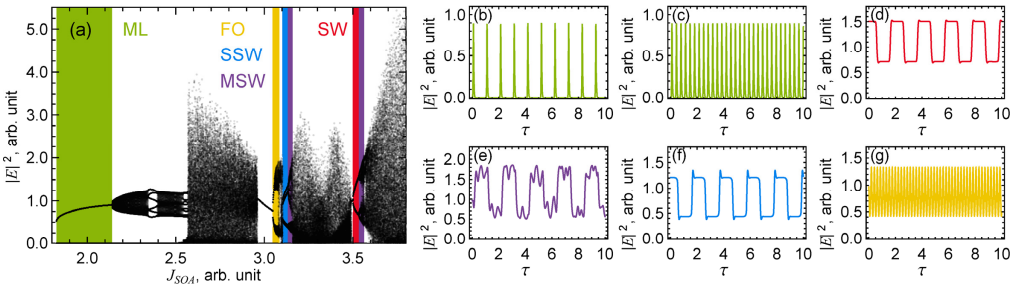

Fig. 3. Numerical simulations proving the hybrid NALM laser reconfigurability. **(a)** Bifurcation diagram showing laser intensity extrema for different operation regimes obtained by varying the SOA gain parameter J_{SOA}, ML – mode-locked regime; MSW – modulated square wave regime; SW – square wave regime; SSW – spike square wave regime; FO – fast oscillation regime. Color plots in (b-g) correspond to those of the areas in (a). **(b)** ML at $J_{\mathrm{SOA}} = 2.1$; **(c)** harmonic ML at $J_{\mathrm{SOA}} = 2.1$; **(d)** SW at $J_{\mathrm{SOA}} = 3.528$; **(e)** MSW at $J_{\mathrm{SOA}} = 3.54$; **(f)** SSW at $J_{\mathrm{SOA}} = 3.131$; **(g)** FO at $J_{\mathrm{SOA}} = 3.055$. The parameters are: $\Gamma = 20$, $\alpha = 0$. The other parameters are the same as in Fig. 2.

For higher SOA gains, when the NALM response is sufficiently nonlinear (the blue line in Fig. 2(a)), the system exhibits square wave (SW) operation. There are two windows of distinguishable dynamical regimes between areas of chaotic oscillations which are characterized by the appearance of SW pulses (Fig. 3(d)), modulated SW oscillations (MSW, Fig. 3(e)), spike SW (SSW, Fig. 3(f)), their harmonics and fast oscillations (FO, Fig. 3(g)). Further increasing the SOA gain invokes quasiperiodic oscillations, and ultimately, chaos. For an SOA gain decrease, the system demonstrates hysteretic behavior, and the sequence of the regimes is the following: chaos, modulated FO, FO, the fifth harmonic of SW, the third harmonic of SW, SW, chaos, MSW, SSW, chaos, quasi-periodic ML, and the second harmonic of ML. The shapes of the SW pulses are only determined by the phase relationship of the lasing modes, and therefore the SW and SSW regimes are dynamically identical and result from the same period-two orbits map in Eq. (3). Therefore, we can conclude on the basis of our theoretical analysis that, experimentally, there are two degrees of freedom we can use to change the system dynamical behavior from traditional ML operation to SW then FO and so on: the SOA gain, which can be adjusted by changing the injection current; the losses and the effective nonlinearity, which can be tuned by means of the polarization controllers.

Optics EXPRESS

As we have mentioned above, the SW operation in our model is mode-locked, and admits harmonics with period as an odd number fraction of the period-two interval. The maximum number of harmonics is defined by the width of the spectral filtering Γ and is bigger for broader filters. For Γ=2000 which is close to the experimental value, it is possible to observe the 51st harmonics of SW, MSW and SSW as shown in Fig. 4. The period of these oscillations corresponds to approximately 1/25th of the cavity roundtrip time.

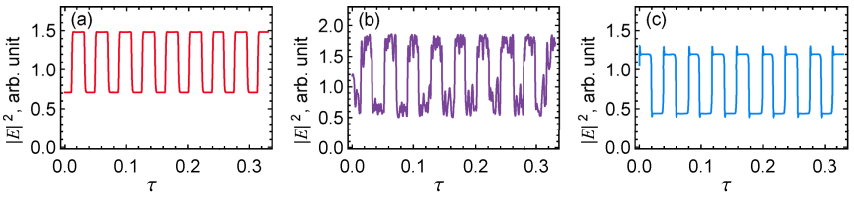

Fig. 4. Numerically obtained harmonics of various square-wave regimes for Γ = 2000: **(a)–(c)** correspond to the regimes (d)–(f) in Fig. 3. The other parameters are the same as in Fig. 3.

4. Experimental results and discussion

The experimental realization for the figure-eight NALM laser architecture is shown in Fig. 1. The nonlinear element, a 45 cm spiral waveguide used in the NALM stage, provides a large nonlinear phase-shift over a short propagation length (characteristic nonlinear length $L_{NL} = 1.7$ km). An advantage of our configuration is that the nonlinearity in the waveguide [33–35] is a few hundred times higher than in previous realizations, typically based on long fiber cavities (see e.g. [36]). The high nonlinearity of the NALM used in the setup enables a sufficient phase shift over a reduced cavity length for the observation of different mode-locked pulse profiles in a single system.

The two polarization controllers, PC1 in the NALM stage and PC2 in the amplifying stage, are used to change both losses and effective nonlinearity. The pulse profiles were detected using a high-speed photo-detector (10 GHz, Lab Buddy DSC-R403) and a high-speed oscilloscope (Agilent, DSO-X 92804A, 28 GHz, sampling rate 10 GSa/s). An optical spectrum analyzer and a RF spectrum analyzer were used to characterize their spectral properties. To experimentally obtain the mode-locking dynamics, we operated the EDFA and the SOA at gain levels of 11 dB and 7.1 dB, respectively. The laser had an active cavity length of 33.8 m, corresponding to a fundamental cavity frequency of $f_r = 7.63$ MHz (round trip time of 131 ns).

Slowly increasing the SOA gain resulted in a passively mode-locked operation featuring a Gaussian pulse profile at the NALM laser threshold of 4.4 dB. Changing the cavity losses and modifying the effective nonlinearity in the NALM through adjusting the polarization controllers PC1 and PC2 or the SOA driving current, allowed switching between different mode-locking regimes. We observed various mode-locked pulse profiles such as ML in Fig. 5(a), HML in Fig. 5(b), SW in Fig. 5(c), SSW in Fig. 5(d), MSW in Fig. 5(e) and FO in Fig. 5(f). The observation can be understood as follows: the adjustment of the polarization controller PC1 allows to increase or decrease the effective losses of the optical field in the waveguide (the quasi TE and TM propagation modes experience different losses), thus leading to continuous changes in the nonlinear phase. The equivalent effect can also be observed by varying the nonlinear phase shift in the NALM stage via the SOA gain. However, the saturation of the SOA gain restricts the nonlinear phase variation, which ultimately constrains the observation of switching between different multistable mode-locked regimes. As evident from Fig. 5(a)–(f), the experimental observations show strong agreement with the theoretical simulated results. The large nonlinear phase-shift emerging from the used waveguide configuration results in a reduction of the amount

Optics EXPRESS

of power required to achieve mode-locking. In particular, we observed mode-locked dynamical states at an average optical output power of ~300 μW (intracavity power ~2.7 mW) with different pulse profiles [37]. We would nevertheless like to mention that by operating the SOA near the NALM laser threshold (SOA = 4.4 dB), we observed the suppression of all dynamical pulse profiles except the ML pulse due to the limited nonlinear phase variations that can be induced at low SOA gains. In contrast, the evolution of the dynamical states shows low sensitivity to the EDFA gain. Incidentally, this is in full agreement with our theoretical findings.

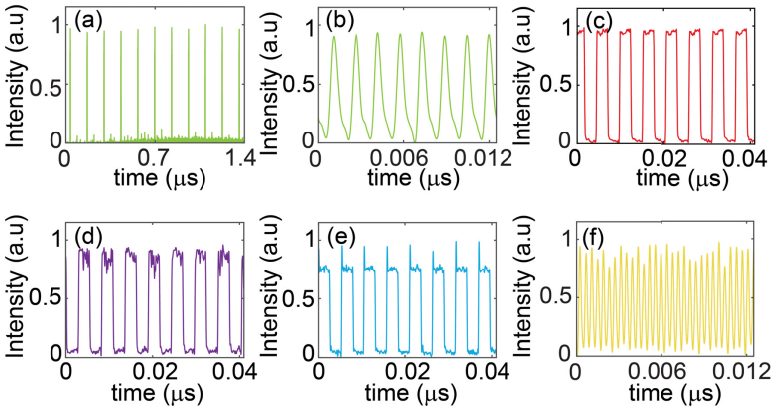

Fig. 5. **(a)** Experimental time traces showing different passively mode-locked dynamical states obtained by varying the polarization controllers PC1 and PC2 for fixed EDFA and SOA gain levels of 11 dB and 2.3 dB, respectively. **(a)–(f)** correspond to the regimes obtained theoretically and shown in Fig. 3 (b)–(g).

For a given SOA current we observe switching between different states by varying the polarization settings. In this case such dynamics emerge from the nonlinear optical NALM response and not from a thermal effect, which is a clear evidence for the optical multistability of the system.

Harmonically mode-locked pulses and SW: Harmonic mode-locking (HML) has been previously reported for the generation of MHz to GHz repetition rate output pulse trains (i.e. few to thousands of harmonics) in the normal dispersion regime or in the dissipative soliton regime [38,39]. This phenomenon relies upon pulse-shaping through gain saturation for the normal dispersive regime, or the soliton peak-power limiting effect for the dissipative soliton resonance regime [39]. Through a simple variation of the polarization controllers, we observe HML (Fig. 5(b)) as well as harmonic mode-locked SWs (Fig. 5(c)–(e)) pulses at judiciously chosen polarization settings. In general, the generation of HML and harmonic mode-locked SW requires high intracavity powers (few hundred mW to W) in order to induce a sufficient nonlinear phase shift [39]. However, the high nonlinearity of the waveguide enables the required nonlinear phase-shifts necessary for high harmonics even at low-power operation. Therefore, we observe HML pulses at milliwatt intracavity powers.

Hysteretic behavior: Similar to other mode-locked lasers based on semiconductor saturable absorbers [29], the NALM laser proposed here shows hysteretic-like behavior among different dynamical states. For the experimental observation of such behavior, we operated the SOA at 4.4 dB, corresponding to the laser operation near the NALM laser threshold for Gaussian-shaped mode-locked pulses. By further increasing the SOA gain parameter while keeping the polarization controllers fixed, we observe various mode locking dynamical states ranging from ML, quasi-ML dynamics, to MSW, SSW, SW pulses for SOA gains of 4.4, 5.3, 6.9, 7.3 and 7.4 dB, respectively. However, when we decrease the SOA current, we observed the states changing from SW to SSW,

Optics EXPRESS

MSW, FO, quasi-ML to ML for SOA gains of 7.4, 7.1, 7.0, 6.8, 6.3 and 5.3 dB, respectively. Such observations clearly show that different pulse profiles correspond to diverse operating values when increasing or decreasing the SOA gain. The hysteretic behavior is caused by the co-existence of multiple stable operation regimes that can be accessed by increasing/decreasing the SOA current, leading to different initial conditions for the adjusted parameter set.

Spectral and temporal characteristics: Let us discuss the formation of SW pulses in nonlinear cavities. There are three formation mechanisms known in the literature: the dissipative soliton resonance (DSR) effect, the noise-like pulses (NLP) mechanism, and the Ikeda instability. For the DSR effect, the SW pulse width can broaden indefinitely when the pump power is increased. Note that the pulse amplitude remains constant. This SW formation effect was theoretically explained in the framework of the cubic-quintic Ginzburg-Landau equation [40,41], but its experimental realization requires strict cavity parameter designs [42]. The DSR phenomenon can always be witnessed with its characteristic Kelly sidebands in the optical spectral profile [43]. In contrast, the NLP mechanism leads to a wave packet consisting of sub-picosecond pulses (with randomly varying amplitude and/or pulse widths), which lack temporal coherence [44,45]. Experimentally, the NLP regime features unusual spikes in the autocorrelation trace [46]. Finally, the formation of a SW through the Ikeda instability is strictly determined by the cavity round trip time [31].

In order to identify the origin of SWs observed in our experiments, we have analyzed the optical spectra, autocorrelation traces and RF spectra for the Gaussian HML, SW, and FO shown in Fig. 6. None of the spectra presents any signs of spectral modulation or Kelly sidebands, which confirms the absence of the DSR effect. The autocorrelation traces for the SW pulses show a constant level over the 200 ps scanning range with no spikes, which confirms that the SW pulse cannot be related to the NLP mechanism.

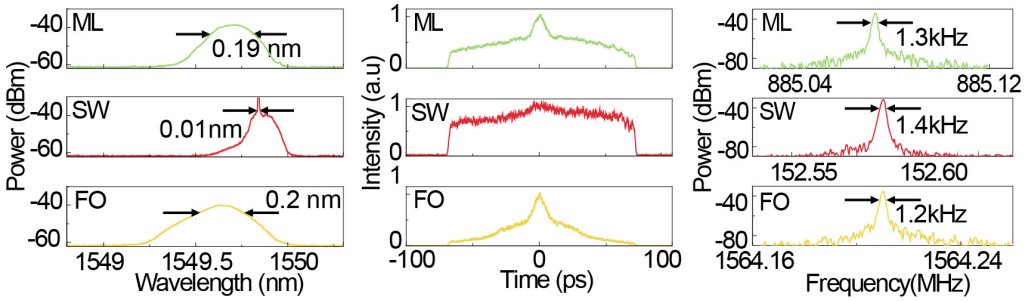

Fig. 6. Experimental optical spectra for different dynamics: harmonic-ML, SW and FO with a central wavelength of ~1550 nm (first column). The corresponding autocorrelation trace (second column). Experimental radio-frequency (RF) spectrum showing clear and narrow peaks at the repetition rate of the dynamical states, confirming stable lasing operation. RF spectrum recorded with a resolution bandwidth (RBW) of 30 Hz, centered at the carrier frequency and with a 1 MHz frequency span (third column).

Therefore, we conclude that the theoretical model based on the DDE (and presented in section 2), fully describes our experimental observations, where the appearance of SW pulses can be related to the Ikeda instability. To the best of our knowledge, this finding has not been reported experimentally for the case of an active nonlinear mode-locked system.

The recorded fundamental RF spectra for different pulse dynamics are shown in Fig. 6 (resolution bandwidth (RBW) of 30 Hz, 1 MHz span, see third column), and have narrow bandwidths in the range of 1.2–1.5 kHz thus confirming stable mode-locked operation. For all mode-locked dynamical regimes, we observe a stable output power of 300 μW over ~20 minutes with a timing jitter of ~12-14 ps, and an SNR of >40. Instabilities associated with the

Optics EXPRESS

optical output can be further minimized to a great extent by incorporating various conventional stabilization techniques [47].

5. Conclusion

We have demonstrated a passively mode-locked laser system, allowing multiple dynamical emission regimes from a single compact architecture. The scheme is based on a NALM configuration including an integrated nonlinear spiral waveguide and a bandpass filter. Our findings show that, by adjusting the nonlinear phase via a polarization-dependent intensity control or the gain via modifying the SOA current, one can achieve various mode-locked optical pulse profiles from one simple setup. We also obtain a variety of different pulse profiles such as higher harmonic mode-locked pulses, square waves, square waves with spikes, modulated square waves and fast oscillations. Differently from previous schemes, and due to the high nonlinearity of the waveguide, the NALM laser presented here shows mode-locking even for very low average power operation (~μW). Our theoretical model, based on a delayed differential equation tailored to a figure-eight laser configuration, well describes the behavior of the observed laser dynamics. We predicted theoretically and confirmed experimentally that the mode-locked SW oscillations originate from the Ikeda instability, and are purely caused by the interplay of gain, losses, and nonlinearity. To the best of our knowledge, this is the first experimental observation of mode-locked SW pulses caused by the Ikeda instability. The numerical results of various mode-locked laser regimes such as Gaussian-like pulses, square-wave pulses, and their harmonics were obtained within a single model based on a delay differential equation approach. The proposed laser configuration, offering a variety of mode-locked pulse profiles in a stable and controlled manner at a reduced power consumption, is a promising solution for many practical applications and can be an all-optical replacement of electronics waveform generators.

Appendix: Derivation of the delay differential equation model

We propose a model for a nonlinear amplifying loop mirror (NALM) laser on the basis of a time-domain lumped element approach [48] by treating the laser components (such as gain media, filters, nonlinear elements) as integral or integro-differential operators acting on the slowly varying complex field amplitude $E(t)$, where t is the local time of the pulse propagating through a dispersion-free ring cavity. We consider the field evolution during the cavity round trip time T in the presence of a bandwidth limiting element. This allows us to transform the delay iteration equation into a delay differential equation (DDE). Experimentally, the optical spectrum consists of more than 10^4 modes which cannot be resolved numerically. We limit our consideration to the case of a narrow filter bandwidth $\Gamma = O(10)$, which also allows adiabatic elimination of the material dynamics, where $O(10)$ denotes the limiting bandwidth value to be in the order of 10 in the numerical simulation [49]. Finally, we assume that counter-propagating fields within the ring cavity do not interact with each other. The SOA and the nonlinear element are placed asymmetrically in the NALM so that in the pulsed operation only one pulse at a time is temporally localized in the element, which avoids interactions.

In Fig. 7, we show the schematic of i) a figure-eight laser with an embedded erbium doped fiber amplifier (EDFA) and ii) a NALM consisting of a semiconductor optical amplifier (SOA) as well as a nonlinear element (NE, e.g. an integrated spiral waveguide or a microring resonator). Here the operators $\hat{K}$, $\hat{G}_{\mathrm{SOA/EDFA}}$, $\hat{D}$ represent the intracavity elements.

In particular, $\hat{D}$ is an operator describing a band-limiting filter which in the frequency domain reads:

$$\hat{D}\tilde{A}(\omega) = \frac{1}{1 - i(\omega - \omega_F)/\Delta}\tilde{A}(\omega), \tag{4}$$

Optics EXPRESS

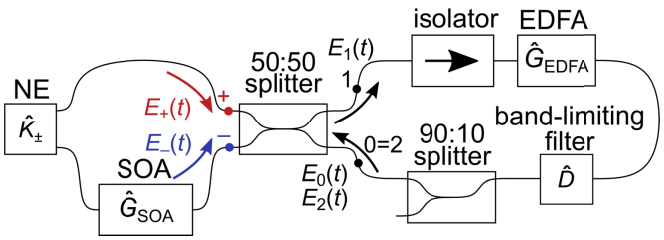

Fig. 7. Schematics of the figure-eight laser based on a nonlinear amplifying loop mirror (NALM). SOA – semiconductor optical amplifier, NE – Kerr-nonlinear element, EDFA – erbium doped fiber amplifier. Propagation in the NALM is characterized by two counter propagating fields as indicated by color arrows. Black arrows show input/output fields at the NALM ports. The points in the scheme have been labeled so to correspond to the field indices in the main text, where further explanations can be found.

where $\tilde{A}(\omega)$ is the Fourier transform of the complex field amplitude $A(t)$; ω is the field frequency; ω_F is the filter transmission peak frequency; and Δ is the filter bandwidth. Note that the frequencies are defined in relation to an arbitrarily chosen cold cavity mode.

Further, $\hat{K}$ is an operator describing a Kerr-type nonlinearity with a phase shift depending (under the assumption of negligible losses) on the input field intensity as [50]:

$$\hat{K}_\pm A(t) = A(t)\exp(-i\gamma_\pm |A(t)|^2), \tag{5}$$

where the indices "+" and "–" correspond to clockwise and counter-clockwise propagation, respectively; $\gamma_\pm$ are the total nonlinear coefficients which account for asymmetry in the nonlinear coefficients due to the opposite propagation directions. This asymmetry is related to the polarization anisotropy of the nonlinear element, as well as to the presence of the polarization controller in one of the NALM arms. We assume, for simplicity, that the polarization anisotropy is negligible, hence $\gamma_+ = \gamma_- = \gamma$, and there is no asymmetry in the nonlinear element operator, so that $\hat{K}_+ = \hat{K}_- = \hat{K}$.

The gain operators $\hat{G}_{SOA}$ and $\hat{G}_{EDFA}$ read:

$$\hat{G}_{SOA}A(t) = A(t)\exp\frac{(1-i\alpha)G_{SOA}(A(t))}{2}, \tag{6}$$

$$\hat{G}_{EDFA}A(t) = A(t)\exp\frac{G_{EDFA}(A(t))}{2}, \tag{7}$$

where $G_{SOA/EDFA}(A) = J_{SOA/EDFA}/(1 + S_{SOA/EDFA}|A|^2)$ are the cumulative SOA and EDFA saturable gains. Here $J_{SOA/EDFA}$ are corresponding small signal gain parameters; $S_{SOA/EDFA}$ are inversely proportional to the saturation intensities; α is the linewidth enhancement factor. Here we assume that the material response of the SOA (~1 ns) is much faster than the timescales determined by the filter and the cavity round-trip time (~0.1 μs), and that the EDFA acts as an almost linear gain element ($S_{EDFA} \ll S_{SOA}$).

Let us consider $E_0(t)$ as the initial field amplitude just before the beam splitter. The two counterpropagating fields inside the NALM can be written as:

$$E_+(t) = \hat{K}\hat{G}_{SOA}\frac{E_0(t)}{\sqrt{2}}, \tag{8}$$

$$E_-(t) = -i\hat{G}_{SOA}\hat{K}\frac{E_0(t)}{\sqrt{2}}, \tag{9}$$

The sequence of operators reflects the different order of elements in which the opposite-direction fields go through when propagating inside the NALM.

Optics EXPRESS

The two counter-propagating fields in the NALM combined at the beam splitter undergo a phase shift given by [51]:

$$E_1(t) = (E_+(t) - iE_-(t))/\sqrt{2}, \tag{10}$$

and after passing through the rest of the cavity the field can be written as:

$$E_2(t) = \sqrt{\kappa}\hat{D}\hat{G}_{\mathrm{EDFA}}E_1(t), \tag{11}$$

where κ is an intensity attenuation coefficient accounting for the reflectivity of the output splitter as well as other linear losses inside the laser cavity.

As we are considering a closed loop configuration, we define point 0 = point 2 (see Fig. 7).

Combining Eqs. (8)–(11), and now replacing $E_2(t) \to E(t)$, $E_0(t) \to E(t-T)$, we can describe the field evolution inside the cavity as a delayed iteration:

$$E(t) = \sqrt{\frac{\kappa}{2}}\hat{D}\hat{G}_{\mathrm{EDFA}}[\hat{K}, \hat{G}_{\mathrm{SOA}}]\frac{E(t-T)}{\sqrt{2}}, \tag{12}$$

where $[\hat{K}, \hat{G}_{\mathrm{SOA}}] \equiv \hat{K}\hat{G}_{\mathrm{SOA}} - \hat{G}_{\mathrm{SOA}}\hat{K}$ is the commutator of the operators $\hat{K}$ and $\hat{G}_{\mathrm{SOA}}$, which describes the interference of two counter-propagating fields outside the NALM. Only the laser off solution $E(t) = 0$ exists if the operators commute, i.e. $[\hat{K}, \hat{G}_{\mathrm{SOA}}] = 0$, due to destructive interference.

The operator $\hat{D}$ expansion leads to a DDE as described in [26]:

$$\Delta^{-1}\dot{E}(t) + E(t) = \sqrt{\frac{\kappa}{2}}\hat{G}_{\mathrm{EDFA}}[\hat{K}, \hat{G}_{\mathrm{SOA}}]\frac{E(t-T)}{\sqrt{2}}, \tag{13}$$

where the dot stands for differentiation with respect to the time t. In Eq. (13) we assume, for the sake of simplicity, that one of the cold cavity frequency modes coincides with the filter peak frequency, which can be shown to lead to the condition $\omega_F = 0$ (again, see [26]).

We expand the operators in Eq. (13) using Eq. (4)–(7) and considering a small gain saturation in the EDFA, and therefore $G_{\mathrm{EDFA}}([\hat{K}, \hat{G}_{\mathrm{SOA}}]E(t-T)) \approx G_{\mathrm{EDFA}}(E(t-T))$:

$$\begin{aligned}\Gamma^{-1}\dot{E}(\tau) + E(\tau) = \tfrac{\sqrt{\kappa}}{2}\exp\tfrac{1}{2}[(1-i\alpha)G_{\mathrm{SOA}}(E(\tau-1))+\\ G_{\mathrm{EDFA}}(E(\tau-1))]\Phi(\tau-1)E(\tau-1),\end{aligned} \tag{14}$$

where dot now means differentiation with respect to the dimensionless time $\tau \equiv t/T$. Here $\Gamma \equiv \Delta T$ is the normalized filter bandwidth; $\Phi(\tau)$ describes the asymmetry-driven nonlinear response of the NALM:

$$\begin{aligned}\Phi(\tau) = \left(1 - \exp\left[-\tfrac{1}{2}i\gamma|E(\tau)|^2(\exp G_{\mathrm{SOA}}(E(\tau)) - 1)\right]\right)\times\\ \exp(-i\gamma|E(\tau)|^2/2).\end{aligned} \tag{15}$$

Funding

Natural Sciences and Engineering Research Council of Canada; Mitacs; Canada Research Chairs; H2020 Marie Skłodowska-Curie Actions (656607); 1000 Talents Sichuan Program; Australian Research Council (DP150104327); Government Council on Grants, Russian Federation (08-08); ITMO University (08-08); Chinese Academy of Sciences (XDB24030000); City University of Hong Kong (9610356).

Acknowledgments

Authors thank G. Huyet and A. G. Vladimirov for fruitful discussions.

Optics EXPRESS

References

1. J. Mandon, G. Guelachvili, and N. Picque, "Fourier transform spectroscopy with a laser frequency comb," Nat. Photonics **3**(2), 99–102 (2009).
2. W. M. Steen and J. Mazumder, *Laser Material Processing* (Springer, 2010).
3. W. Shi, Q. Fang, X. Zhu, R. A. Norwood, and N. Peyghambarian, "Fiber lasers and their applications," Appl. Opt. **53**(28), 6554–6568 (2014).
4. U. Keller, "Recent developments in compact ultrafast lasers," Nature **424**(6950), 831–838 (2003).
5. H. A. Haus, "Mode-locking of lasers," IEEE J. Sel. Top. Quantum Electron. **6**(6), 1173–1185 (2000).
6. E. P. Ippen, "Principles of passive mode locking," Appl. Phys. B **58**(3), 159–170 (1994).
7. M. E. Fermann, F. Haberl, M. Hofer, and H. Hochreiter, "Nonlinear amplifying loop mirror," Opt. Lett. **15**(13), 752–754 (1990).
8. J. C. Hernandez-Garcia, O. Pottiez, R. Grajales-Coutiño, B. Ibarra-Escamilla, E. A. Kuzin, J. M. Estudillo-Ayala, and J. Gutierrez-Gutierrez, "Generation of long broadband pulses with a figure-eight fiber laser," Laser Phys. **21**(8), 1518–1524 (2011).
9. M. Nakazawa, E. Yoshida, and Y. Kimura, "Low threshold, 290 fs erbium-doped fiber laser with a nonlinear amplifying loop mirror pumped by InGaAsP laser diodes," Appl. Phys. Lett. **59**(17), 2073–2075 (1991).
10. M. Kues, C. Reimer, B. Wetzel, P. Roztocki, B. E. Little, S. T. Chu, T. Hansson, E. A. Viktorov, D. J. Moss, and R. Morandotti, "Passively mode-locked laser with an ultra-narrow spectral width," Nat. Photonics **11**(3), 159–162 (2017).
11. J. P. Lauterio-Cruz, J. C. Hernandez-Garcia, O. Pottiez, J. M. Estudillo-Ayala, E. A. Kuzin, R. Rojas-Laguna, H. Santiago-Hernandez, and D. Jauregui-Vazquez, "High energy noise-like pulsing in a double-clad Er/Yb figure-of-eight fiber laser," Opt. Express **24**(13), 13778–13787 (2016).
12. D. Chaparro, L. Furfaro, and S. Balle, "Subpicosecond pulses in a self-starting mode-locked semiconductor-based figure-of-eight fiber laser," Photonics Res. **5**(1), 37–40 (2017).
13. T. P. Montoya and G. S. Smith, "Land mine detection using a ground-penetrating radar based on resistively loaded vee dipoles," IEEE Trans. Antennas Propag. **47**(12), 1795–1806 (1999).
14. S. W. Hell and J. Wichmann, "Breaking the diffraction resolution limit by stimulated emission: stimulated-emission-depletion fluorescence microscopy," Opt. Lett. **19**(11), 780–782 (1994).
15. M. Sheik-Bahae, A. A. Said, T. H. Wei, D. J. Hagan, and E. W. Van Stryland, "Sensitive measurement of optical nonlinearities using a single beam," IEEE J. Quantum Electron. **26**(4), 760–769 (1990).
16. R. Kaiser and B. Hüttl, "Monolithic 40-GHz mode-locked MQW DBR lasers for high-speed optical communication systems," IEEE J. Sel. Top. Quantum Electron. **13**(1), 125–135 (2007).
17. P. Roztocki, M. Kues, C. Reimer, B. Wetzel, S. Sciara, Y. Zhang, A. Cino, B. E. Little, S. T. Chu, D. J. Moss, and R. Morandotti, "Practical system for the generation of pulsed quantum frequency combs," Opt. Express **25**(16), 18940–18949 (2017).
18. A. M. Kaplan, G. P. Agrawal, and D. N. Maywar, "Optical square-wave clock generation based on an all-optical flip-flop," IEEE Photonics Technol. Lett. **22**(7), 489–491 (2010).
19. W. Chang, A. Ankiewicz, J. M. Soto-Crespo, and N. Akhmediev, "Dissipative soliton resonances," Phys. Rev. A **78**(2), 023830 (2008).
20. I. A. Young, J. K. Greason, and K. L. Wong, "A PLL clock generator with 5 to 110 MHz of lock range for microprocessors," IEEE J. Solid-State Circuits **27**(11), 1599–1607 (1992).
21. P. Grelu and N. Akhmediev, "Dissipative solitons for mode-locked lasers," Nat. Photonics **6**(2), 84–92 (2012).
22. A. Pasquazi, Y. Park, J. Azaña, F. Légaré, R. Morandotti, B. E. Little, S. T. Chu, and D. J. Moss, "Efficient wavelength conversion and net parametric gain via Four Wave Mixing in a high index doped silica waveguide," Opt. Express **18**(8), 7634–7641 (2010).
23. A. Pasquazi, M. Peccianti, Y. Park, B. E. Little, S. T. Chu, R. Morandotti, J. Azaña, and D. J. Moss, "Sub-picosecond phase-sensitive optical pulse characterization on a chip," Nat. Photonics **5**(10), 618–623 (2011).
24. D. J. Moss, R. Morandotti, A. L. Gaeta, and M. Lipson, "New CMOS-compatible platforms based on silicon nitride and Hydex for nonlinear optics," Nat. Photonics **7**(8), 597–607 (2013).
25. R. T. Deck, M. Mirkov, and B. G. Bagley, "Determination of bending losses in rectangular waveguides," J. Lightwave Technol. **16**(9), 1703–1714 (1998).
26. A. G. Vladimirov, D. Turaev, and G. Kozyreff, "Delay differential equations for mode-locked semiconductor lasers," Opt. Lett. **29**(11), 1221–1223 (2004).
27. A. G. Vladimirov, A. V. Kovalev, E. A. Viktorov, N. Rebrova, and G. Huyet, "Dynamics of a class A nonlinear mirror mode-locked laser," Phys. Rev. E **100**(1), 012216 (2019).
28. C. Henry, "Theory of the linewidth of semiconductor lasers," IEEE J. Quantum Electron. **18**(2), 259–264 (1982).
29. M. Marconi, J. Javaloyes, S. Balle, and M. Giudici, "How lasing localized structures evolve out of passive mode locking," Phys. Rev. Lett. **112**(22), 223901 (2014).
30. A. V. Kovalev and E. A. Viktorov, "Class-A mode-locked lasers: Fundamental solutions," Chaos **27**(11), 114318 (2017).
31. K. Ikeda, K. Kondo, and O. Akimoto, "Successive higher-harmonic bifurcations in systems with delayed feedback," Phys. Rev. Lett. **49**(20), 1467–1470 (1982).

Optics EXPRESS

32. M. W. Derstine, H. M. Gibbs, F. A. Hopf, and D. L. Kaplan, "Alternate paths to chaos in optical bistability," Phys. Rev. A **27**(6), 3200–3208 (1983).
33. D. Duchesne, M. Peccianti, M. R. Lamont, M. Ferrera, L. Razzari, F. Légaré, R. Morandotti, S. T. Chu, B. E. Little, and D. J. Moss, "Supercontinuum generation in a high index doped silica glass spiral waveguide," Opt. Express **18**(2), 923–930 (2010).
34. D. Duchesne, M. Ferrera, L. Razzari, R. Morandotti, B. E. Little, S. T. Chu, and D. J. Moss, "Efficient self-phase modulation in low loss, high index doped silica glass integrated waveguides," Opt. Express **17**(3), 1865–1870 (2009).
35. Y. Zhang, C. Reimer, J. Wu, P. Roztocki, B. Wetzel, B. E. Little, S. T. Chu, D. J. Moss, B. J. Eggleton, M. Kues, and R. Morandotti, "Multichannel phase-sensitive amplification in a low-loss CMOS-compatible spiral waveguide," Opt. Lett. **42**(21), 4391–4394 (2017).
36. Z. B. Lin, A. P. Luo, S. K. Wang, H. Y. Wang, W. J. Cao, Z. C. Luo, and W. C. Xu, "Generation of dual-wavelength domain-wall rectangular shape pulses in HNLF-based fiber ring laser," Opt. Laser Technol. **44**(7), 2260–2264 (2012).
37. A. B. Grudinin, D. J. Richardson, and D. N. Payne, "Energy quantisation in figure eight fibre laser," Electron. Lett. **28**(1), 67–68 (1992).
38. H. R. Chen, K. H. Lin, C. Y. Tsai, H. H. Wu, C. H. Wu, C. H. Chen, Y. C. Chi, G. R. Lin, and W. F. Hsieh, "12 GHz passive harmonic mode-locking in a 1.06 μm semiconductor optical amplifier-based fiber laser with figure-eight cavity configuration," Opt. Lett. **38**(6), 845–847 (2013).
39. Y. Wang, J. Li, K. Mo, Y. Wang, F. Liu, and Y. Liu, "14.5 GHz passive harmonic mode-locking in a dispersion compensated Tm-doped fiber laser," Sci. Rep. **7**(1), 7779 (2017).
40. G. Semaan, F. B. Braham, J. Fourmont, M. Salhi, F. Bahloul, and F. Sanchez, "10 μJ dissipative soliton resonance square pulse in a dual amplifier figure-of-eight double-clad Er: Yb mode-locked fiber laser," Opt. Lett. **41**(20), 4767–4770 (2016).
41. X. Zhang, C. Gu, G. Chen, B. Sun, L. Xu, A. Wang, and H. Ming, "Square-wave pulse with ultra-wide tuning range in a passively mode-locked fiber laser," Opt. Lett. **37**(8), 1334–1336 (2012).
42. S. M. Kelly, "Characteristic sideband instability of periodically amplified average soliton," Electron. Lett. **28**(8), 806–807 (1992).
43. J. Liu, Y. Chen, P. Tang, C. Xu, C. Zhao, H. Zhang, and S. Wen, "Generation and evolution of mode-locked noise-like square-wave pulses in a large-anomalous-dispersion Er-doped ring fiber laser," Opt. Express **23**(5), 6418–6427 (2015).
44. A. F. Runge, G. Aguergaray, N. G. Broderick, and M. Erkintalo, "Coherence and shot-to-shot spectral fluctuations in noise-like ultrafast fiber lasers," Opt. Lett. **38**(21), 4327–4330 (2013).
45. H. Chen, S. Chen, Z. Jiang, and J. and Hou, "0.4 μJ, 7 kW ultrabroadband noise-like pulse direct generation from an all-fiber dumbbell-shaped laser," Opt. Lett. **40**(23), 5490–5493 (2015).
46. Z. S. Deng, G. K. Zhao, J. Q. Yuan, J. P. Lin, H. J. Chen, H. Z. Liu, A. P. Luo, H. Cui, Z. C. Luo, and W. C. Xu, "Switchable generation of rectangular noise-like pulse and dissipative soliton resonance in a fiber laser," Opt. Lett. **42**(21), 4517–4520 (2017).
47. X. Shan and D. M. Spirit, "Spirit "Novel method to suppress noise in harmonically mode-locked erbium fibre lasers," Electron. Lett. **29**(11), 979–981 (1993).
48. E. Avrutin and J. Javaloyes, "Mode-locked Semiconductor Lasers," in *Handbook of Optoelectronic Device Modeling and Simulation. Volume 2*, J. Piprek, ed. (CNC, 2018), pp. 187–210.
49. T. H. Cormen, E. L. Charles, R.L. Rivest, and C. Stein, "*Introduction to algorithms*" 2nd ed. (MIT, 2001).
50. G. P. Agrawal, *Nonlinear Fiber Optics* (Academic, 2013).
51. A. Takagi, K. Jinguji, and M. Kawachi, "Wavelength Characteristics of (2 (2) Optical Channel-Type Directional Couplers with Symmetric or Nonsymmetric Coupling Structures," J. Lightwave Technol. **10**(6), 735–746 (1992).